

Heart Rate Estimation based on Optical Flow: Enabling Smooth Angle Changes in Ultrasound Simulation

Henning Schäfer^{1,2}^a, Hendrik Damm^{1,3}^b and Christoph M. Friedrich^{1,4}^c

¹Department of Computer Science, University of Applied Sciences and Arts Dortmund (FHDO), Dortmund, NRW, Germany

²Institute for Transfusion Medicine, University Hospital Essen, Essen, NRW, Germany

³Institute of Epidemiology and Social Medicine, University of Münster, Münster, NRW, Germany

⁴Institute for Medical Informatics, Biometry and Epidemiology (IMIBE), University Hospital Essen, Essen, NRW, Germany

Keywords: Biomedical Image Processing, Ultrasound Imaging, Vascular Imaging, Image Visualization, Functional Image Analysis, 3D Video-based Ultrasound Simulation.

Abstract: Ultrasound simulators show previously recorded ultrasound videos from different angles to the trainee. During acquisition, breathing, pulse, and other motion artifacts are involved, which often prevent a smooth image transition between different angles during simulation. In this work, a global motion vector is derived using the Lucas–Kanade method for calculating the optical flow in order to create a motion profile in addition to the recording. This profile allows transition synchronization in ultrasound simulators. For the transition in kidney recordings, the Pearson’s r correlation could be increased from 0.252 to 0.495 by autocorrelating motion profiles and synchronizing them based on calculated delays. Approaches based on tracking and structural similarity were also evaluated, yet these have shown inferior qualitative transition results. In ultrasound videos with visibility of vessels, e.g., thyroid gland with carotid artery or echocardiogram, the heart rate can also be estimated via the optical flow. In the abdominal region, the signal contains respiratory information. Since the motion profile can be generated in real time directly at the transducer position, it could be useful for diagnostic purposes.

1 INTRODUCTION

An ultrasound simulator is a medical simulation training device that enables trainees to practice diagnostic, therapeutic, and surgical applications related to ultrasound-based imaging techniques. To achieve these training results, simulators mimic the ultrasound image. An ultrasound simulator, 3D video-based, shows previously recorded ultrasound videos from different angles. When the trainee moves the transducer, e.g., an imitation with a gyroscope sensor, transitions should be made between the recordings from the different angles so that a realistic scenario of the sounding of an organ can be reproduced. During angle transition, hard image jumps can occur (see Figure 1). This is because of respiration, pulse, and other motion artifacts that were recorded at the time of acquisition. Here, a structures to be observed jumps

further (see previous position based on red line), because the asynchronous angle change causes the respiration to be in a different cycle. In order to prevent these jumps during simulation, a synchronization of the recordings from the different angles is needed. The objective of this work is to apply and evaluate different methods to investigate their suitability for synchronizing ultrasound acquisitions from different angles. An overview on other approaches for ultrasound simulators can be seen in (Ourahmoune et al., 2012; Blum et al., 2013). Starting from an arbitrary frame of one angle, the best matching frame from the target angle is to be selected, so that there are minimal artifacts as possible during transition. Both angles need to be synchronized with respect to respiration and pulse. Previous approaches to synchronize the images by recording the respiration and the pulse could not always enable a smooth change. The abdominal region, where vascular and thoracic respiratory motion affect the ultrasound image, is considered to be challenging. For this work, videos of organs were acquired at different angles. These are each

^a  <https://orcid.org/0000-0002-4123-0406>

^b  <https://orcid.org/0000-0002-7464-4293>

^c  <https://orcid.org/0000-0001-7906-0038>

10 seconds long and have a frame count of 30 frames per second. They are to be displayed to the trainee in a continuous loop to simulate a real ultrasound image. A transducer mockup with a gyroscope is used to estimate its angle for selection of the respective imaging output from recordings. In the case of a change of angle, transitions occur, which are to be synchronized by means of different approaches, which are presented in this work.

In the remainder of this paper, Section 2 provides a short overview of related work and state of the art approaches. Section 3 describes the methods used in this paper. In Section 4 the obtained results are evaluated and finally concluded afterwards in Section 5.



Figure 1: Transition through a kidney examination, (a) shows imaging output at 90° , (b) shows imaging output at 95° with a motion artifact due to respiration (marked in red).

2 RELATED WORK

This section describes related work used for synchronization approaches.

2.1 Optical Flow

Optical flow is a commonly used method for motion estimation in a scene with a wide range of applications. Many gradient-based methods such as the Horn-Schunck method (Horn and Schunck, 1981) and the Lucas-Kanade method (Lucas and Kanade, 1981) have been developed to estimate optical flow based on the calculation of brightness gradients.

In the gradient-based methods, partial derivatives with respect to temporal coordinates are calculated as brightness gradients (Kearney et al., 1987). As soon as objects in a scene move with high velocities, the gradient-based methods are less suitable (Lawton, 1983). Gradient-based optical flow methods, unlike correlation-based flow methods (Bergen et al., 1990; Lawton, 1983) can be computed more quickly and are suitable for real-time estimation of optical flow. The Lucas-Kanade method is a widely used differential method for estimating optical flow proposed by Bruce D. Lucas and Takeo Kanade (Lucas and

Kanade, 1981). It assumes that the optical flow in the neighborhood of the pixel is a constant, and then uses the least squares method to solve the basic equation of optical flow for all pixels in the neighborhood.

2.2 Structural Similarity

From a study on tracking in ultrasound images of the tongue (Xu et al., 2016), the Complex Wavelet Structural Similarity Index (CW-SSIM) behaves uniformly and predictably for slight rotations in ultrasound images. To this end, different metrics for calculating similarity were compared for rotations ranging from -10° to $10^\circ+$ in an ultrasound image.

The Structural Similarity Index (SSIM) is a method for measuring the similarity between two images (Wang et al., 2004). The index is often understood as a quality measure against the image to be compared, e.g. altered by noise.

The metric is based on the assumption that the human visual system (HVS) model is more responsive to structural changes. Therefore, a measure that quantifies structural similarity should be a good approximation of the actual changes perceived by the HVS.

The CW-SSIM index (Sampat et al., 2009) is an extension of the SSIM to the complex wavelet domain, which is more robust to certain image changes (e.g., translation and rotation).

2.3 Tracking

During the tracking approach, various frames of an angle should be downstreamed at random intervals to verify that tracking of the structure continues. The assumption is that if the tracking of a structure can be continued successfully, there is a smooth change of angle.

The Discriminative Correlation Filter with Channel and Spatial Reliability (DCF-CSR) is a tracking method for short-term tracking of structures (Bolme et al., 2010; Lukežič et al., 2018). Here, tracking using Correlation Filter has been extended to DCF tracking by the concepts of channel and spatial reliability. Spatial reliability adjusts filter support to the region of the object selected for tracking. This allows both an increase in search area and better tracking of non-rectangular objects (Lukežič et al., 2018).

With only two features, histogram of oriented gradients (HoGs) and colornames, the CSR-DCF method achieves state-of-the-art results on several tracking challenges (VOT 2016, VOT 2015, and OTB100) (Matej et al., 2016; Roffo et al., 2016; Wu et al., 2015). The CSR-DCF runs in real-time on a CPU.

2.4 Heart Rate Estimation

One way of enriching the ultrasound images with further information is to indicate the heart rate. If this was not recorded at the time of acquisition, it can be reconstructed by visual image processing. Theoretically, this possibility exists whenever image areas of the ultrasound are directly or indirectly exposed to changes caused by the expansion of blood vessels. Puybureau et al. (Puybureau et al., 2015) use fish embryos to show that the optical flow of blood vessels in the heart can be used to reconstruct the pulse. Furthermore, a distinction between artery and vein could be derived from clustering of the speed vectors. Boukerroui et al. (Boukerroui et al., 2003) show that the movement of the endocardium (innermost layer of the heart wall) in the left ventricle can be tracked based on ultrasound images using velocity estimation. The movements of the left ventricle were recorded over time similar to the tracking of fish embryo vessels (Puybureau et al., 2015).

3 METHODS

The approaches described in Section 2, namely optical flow (see Section 3.1), CW-SSIM (see Section 3.3), and tracking with DCF-CSR (see Section 3.2), will be applied to different ultrasound recordings. For this purpose, videos of the kidney, thyroid and different views of the heart (echocardiography)¹, as well as the abdomen (gallbladder) will be used. Except for the cardiac ultrasound, all recordings for this work were acquired in 30 FPS and are always 10 seconds long². For each image, there is a corresponding angle spectrum from approximately -30° to $+30^\circ$ in 5° degree steps (see Figure 2).

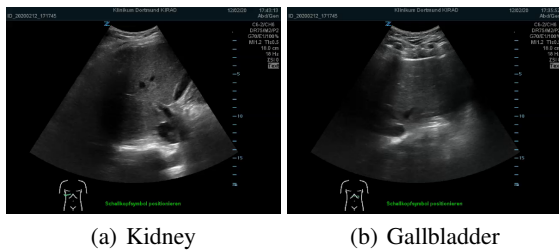


Figure 2: (a) Image of the kidney with structures partially moving due to pulse and respiration, (b) Image of the gallbladder with movement of the abdomen due to respiration.

¹Echocardiography views were taken from https://youtu.be/2XR6etAY_-w, last accessed: 07.11.2021
²Acquired from ZONARE ZS3, C6-2, convex transducer, 2-6 MHz.

3.1 Optical Flow Calculation via Lucas–Kanade

The Lucas-Kanade method is used to approximate the optical flow. For this purpose, the original image is divided into smaller sections. The basic calculation of the algorithm (Lucas and Kanade, 1981; Ishii et al., 2011) is shown in equation (1).

$$I_t + v_x I_x + v_y I_y = 0 \quad (1)$$

$I(x, y, t)$ describes the brightness of a pixel at position (x, y) at time t . If $I(x, y, t)$ does not change excessively between frames, the optical flow can be calculated using equation (1), where I_x , I_y and I_t are the partial derivatives of $I(x, y, t)$ resolved to x , y and t . v_x and v_y describe the *velocity*, i.e., the momentum of motion associated with the optical flow of $I(x, y, t)$. It is now assumed that v_x and v_y remain constant over a smaller range, from which equation (2) is derived (Ishii et al., 2011).

$$\begin{aligned} S_{xx}v_x + S_{xy}v_y + S_{xt} &= 0 \\ S_{xy}v_x + S_{yy}v_y + S_{yt} &= 0 \end{aligned} \quad (2)$$

Where S_{xx} , S_{xy} , S_{yy} , S_{xt} and S_{yt} are the product sums of the partial derivatives of I_x , I_y and I_t in the constant small range Γ (shown in equation (3)) (Ishii et al., 2011).

$$\begin{aligned} S_{xx} &= \sum_{\Gamma} I_x I_x, S_{xy} = \sum_{\Gamma} I_x I_y, S_{yy} = \sum_{\Gamma} I_y I_y \\ S_{xt} &= \sum_{\Gamma} I_x I_t, S_{yt} = \sum_{\Gamma} I_y I_t \end{aligned} \quad (3)$$

The velocity in x and y direction can be calculated by solving equation (2) over equation (4) (Ishii et al., 2011).

$$\begin{pmatrix} v_x \\ v_y \end{pmatrix} = \begin{pmatrix} \frac{S_{yy}S_{xt} - S_{xy}S_{yt}}{S_{xx}S_{yy} - S_{xy}^2} \\ \frac{-S_{xy}S_{xt} + S_{xx}S_{yt}}{S_{xx}S_{yy} - S_{xy}^2} \end{pmatrix} \quad (4)$$

By using the velocity vectors v_x , v_y the movement of pixels with constant brightness of a region is obtained. Since in ultrasound images the intensity of structures does not change much and therefore strong jumps are not to be expected, the Lucas-Kanade method is considered to be suitable for estimating optical flow.

3.1.1 Global Motion Profile Generation via Lucas–Kanade

In order to smoothly change the angle between the recordings of an organ at any frame, a global motion profile is to be generated. For this purpose, the velocity of a zone is calculated for each frame in comparison to the previous frame.

To optimize the calculation, the image is divided into 8×8 zones. The size of the zone depends on the resolution of the ultrasound recording. Since the motion profile can be preprocessed for the transitions, small zones at high resolution are also possible. Here, the distribution of apparent velocities in direction u and v yields an average *movement of brightness pattern* D (Du_{xy} and Dv_{xy}) of a 8×8 pixel zone at time t_1 .

The idea for motion profiling is now based on the fact that the average of all *movements* within a frame gives a global motion tendency DG of the optical flow (DG_u and DG_v) (see equation (5)), where k stands for the number of all 8×8 regions in an ultrasound frame.

$$\begin{pmatrix} DG_u \\ DG_v \end{pmatrix} = \begin{pmatrix} \frac{\sum^k Du_{xy}}{k} \\ \frac{\sum^k Dv_{xy}}{k} \end{pmatrix} \quad (5)$$

The global movement of brightness DG_u and DG_v measured over the duration of the recording gives the motion profile of an ultrasound video. Figure 3 shows such a motion profile to an echocardiogram recorded over 3 seconds of DG in the direction u , the movement on the horizontal axis. Figure 4 shows DG in the v direction, the movement on the vertical axis.

3.1.2 Heart Rate Estimation via Global Motion Profiles

To estimate the heart rate from a raw optical flow signal, the Pan-Tompkins method (Pan and Tompkins, 1985) is used. The Pan-Tompkins method applies a series of filters to emphasize the frequency content of the cardiac depolarization.

The values determined by optical flow are the velocity values in m/s from equation (5). Due to the adaptive threshold, the algorithm should still be able to reliably detect an edge from the raw signal, provided that a vessel is recorded.

3.2 Discriminative Correlation Filter with Channel and Spatial Reliability

Tracking of structures is also a possible approach to prevent image jumps during changeover. The structures changing due to respiration and pulse over the period of the ultrasound recording could be recognized in the frames of the recording of the next angle.

Here, out of all the frames in which tracking can be continued, the frame with the smallest distance of the tracked area from the original frame is assumed to achieve a continuation of the natural motion. The `opencv` (Bradski, 2000) implementation was used.

3.3 Complex Wavelet Structural Similarity

For this method, a random frame was taken from the recordings of a kidney (source frame) and compared with all possible frames in the next angle of the ultrasound recording using the Similarity Index (CWSSIM).

4 EVALUATION

The presented methods have been evaluated with respect to their suitability for smooth angle changes in ultrasound simulators.

4.1 Optical Flow

To enable synchronized angle changes, the optical flow motion profiles of different angles on ultrasound images of a same organ are assumed to be signals that correlate with themselves at an earlier time. These recurrent movements, e.g., due to respiration, can therefore be synchronized by determining the lag to an adjacent angle.

For example, in the ultrasound simulator the recording is permanently shown from angle 90 degrees. If the trainee decides to change the view to 95 degrees, the lag is resolved via autocorrelation (Bracewell, 1978), resulting in a synchronous change. For this purpose, the lag to the pre-signal is compensated and the result is translated into the appropriate frame on the time axis, so that the new image continues e.g. at the same time of the breathing phase. The synchronization of the angle changes by the motion profiles in horizontal and vertical direction by means of shifting the lag was tested by carrying out angle changes at random time, in each case with and without synchronization. Without synchronization, structures of the ultrasound image suddenly appear at other positions after the change, because they have shifted at the time of acquisition, e.g. due to respiration or pulse. Such a jump can be seen in Figure 1. With synchronization, it is also clearly visible that the angle has changed, but the moving structures to be observed are continued in their movement, resulting in a smooth change.

The application of the signals of two angles aligned by the determined lag through autocorrelation (see Figure 8) can be seen in Figure 9. After shifting by the compensated lag, these result in a synchronized motion profile. To ensure that the motion profile contains valuable information, profiles of recordings with

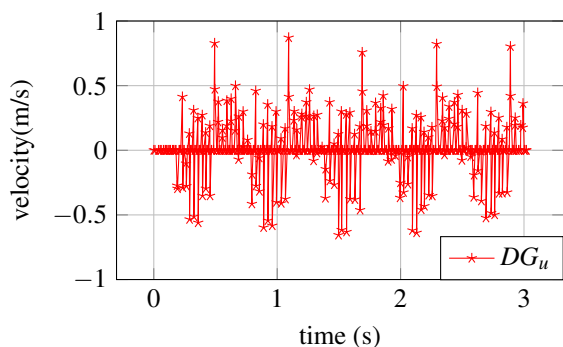


Figure 3: Global movement DG as velocity (m/s) in direction u (horizontal axis) determined in an echocardiogram measured over time (s).

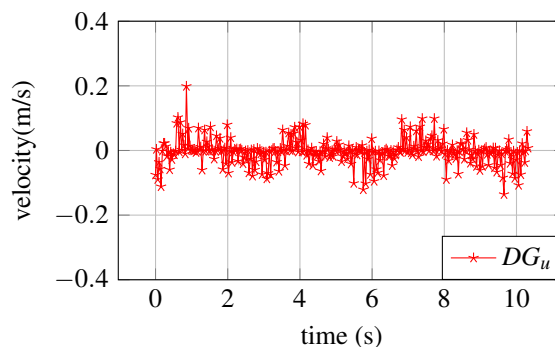


Figure 5: Global movement DG as velocity (m/s) in direction u (horizontal axis) determined in the abdomen (gallbladder) measured over time (s).

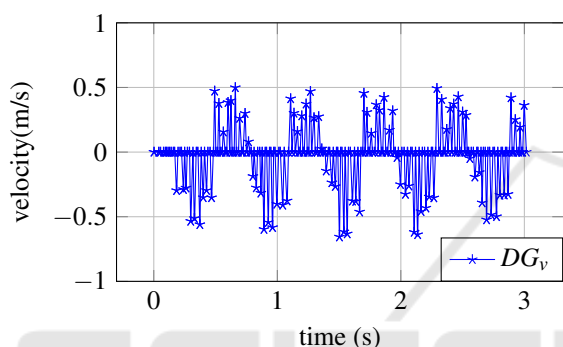


Figure 4: Global movement DG as velocity (m/s) in direction v (vertical axis) determined in an echocardiogram measured over time (t).

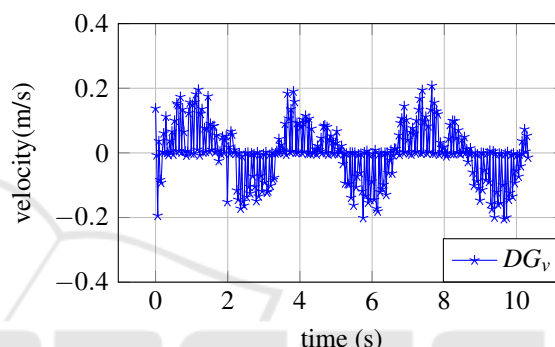


Figure 6: Global movement DG as velocity (m/s) in direction v (vertical axis) determined in the abdomen (gallbladder) measured over time (s). Here visible, the 3-fold respiratory cycle.

movements through vessels as well as through respiration were generated. Figure 3 shows the global movement DG as velocity (m/s) in direction u (horizontal axis) determined in an echocardiogram measured over time (t). Figure 4 shows the recording correspondingly in vertical axis. The 3-second recording is from the coronary venous sinus view of the heart. Here, the heart rate of 5 beats in 3 seconds is visible on both axes and can be read visually. The motion profile could also be interpreted well in other views such as the full view (four chamber view) or the mitral valve.

For organs in the abdominal region, such as the gallbladder, the expansion of the thorax due to respiration is the main factor for movements in the ultrasound image. Figure 5 shows the global movement DG in horizontal axis determined in the abdomen (gallbladder) measured over a period of about 10 seconds. Here, the motion is not visible because the acquisition was horizontal and therefore the respiratory motion is mainly in the direction of the vertical axis.

Figure 6 shows the global movement DG in vertical axis. The respiratory cycle can be read well. In the period of 10 seconds, 3 respiratory cycles took place.

4.1.1 Heart Rate Estimation

Figure 7 shows the estimation of heart rate with the Pan-Tompkins method (blue markers). Here, an ultrasound video of the aorta was used to determine optical flow.

The optical flow was smoothed with a Gaussian filter and then overlaid with data obtained from a pulse oximeter worn on the left index finger. The pulse was recorded synchronously in addition to the optical flow during ultrasound acquisition. The optical flow and the pulse curve correlate with each other.

The adaptive threshold allows the algorithm to perform edge detection from the raw signal and estimate the heart rate by counting detected peaks, provided a vessel is recorded.

4.2 Tracking with DCF-CSR

For this experiment, several images of the kidney were chosen with smaller artifacts that change with respiration and/or pulse. During tracking, different frames of an applied angle were then downstreamed

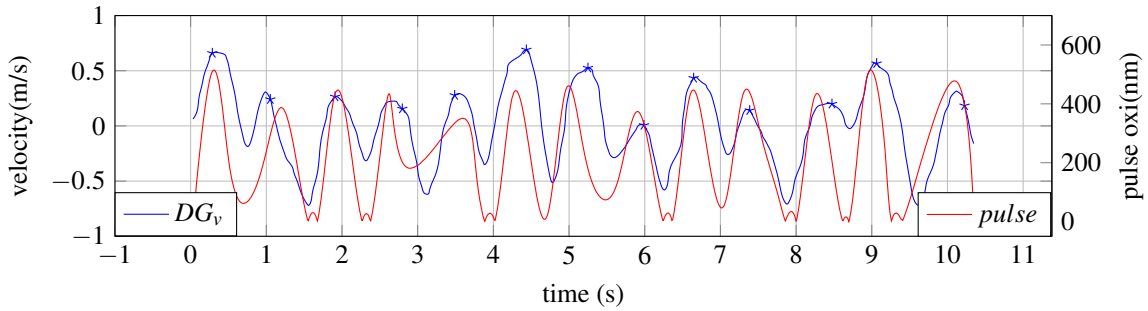


Figure 7: Estimation of heart rate using Pan-Tompkins method on the raw signal of the motion profile and the pulse oximeter for validation (in this case, ultrasound of the aorta on the vertical axis).

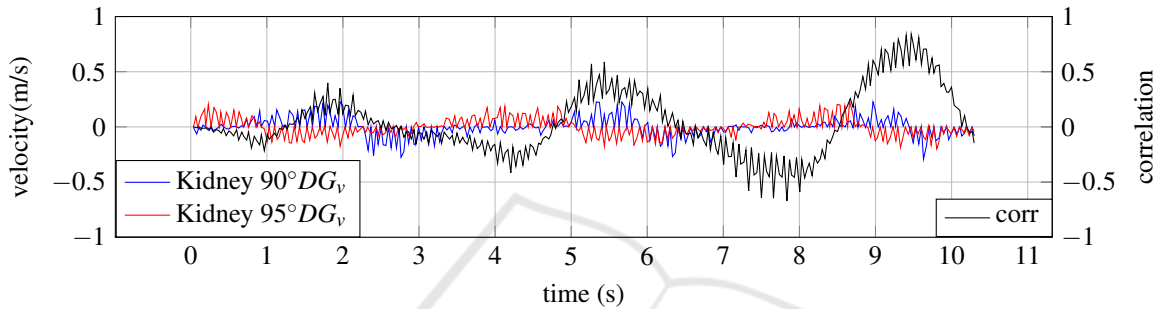


Figure 8: Vertical motion profiles of ultrasound recordings of the kidney at two different angles and the corresponding cross-correlation. A lag of 3 seconds in the respiratory cycle at the two angles results from the different start times of the ultrasound acquisition and can be seen in the motion profile here. Pearson r correlation coefficient between both angles (without resolving lag) is 0.252.

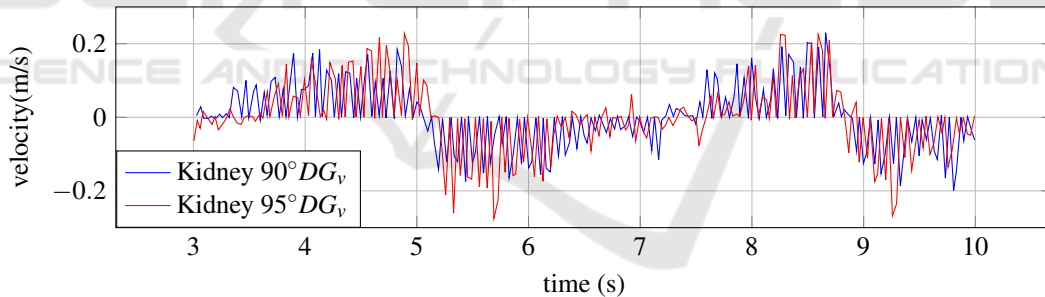


Figure 9: Synchronized motion profile, shifted over lag determined by autocorrelation. By compensating for lag, the moving structures to be observed are continued in their movement. In this example, pearson r correlation increases from 0.252 to 0.4953 by synchronizing the lag.

at randomly selected intervals to check whether the tracking of the structure can be continued.

Since the search range in DCF-CSR is very high, errors often occurred and another structure was continued. Tracking beyond the angle change is error-prone, as the object may no longer be visible. The carotid artery near the thyroid gland could be tracked well, but not with sufficiently high FPS. Accordingly, the tracking would have to be preprocessed.

This approach also lacks the tendency of the movement, i.e. the position of the object can be at the same place e.g. when exhaling and inhaling with

a different momentum each time, but this is not considered in the search range of the tracking in the new angle.

4.3 Frame Comparison with CW-SSIM

For this experiment, a random frame was taken from the image of a kidney (source frame) and compared with all possible frames in the next angle of the ultrasound image using the Similarity Index (CW-SSIM). The structure of interest moved horizontally during the acquisition, so it is necessary to find a frame that

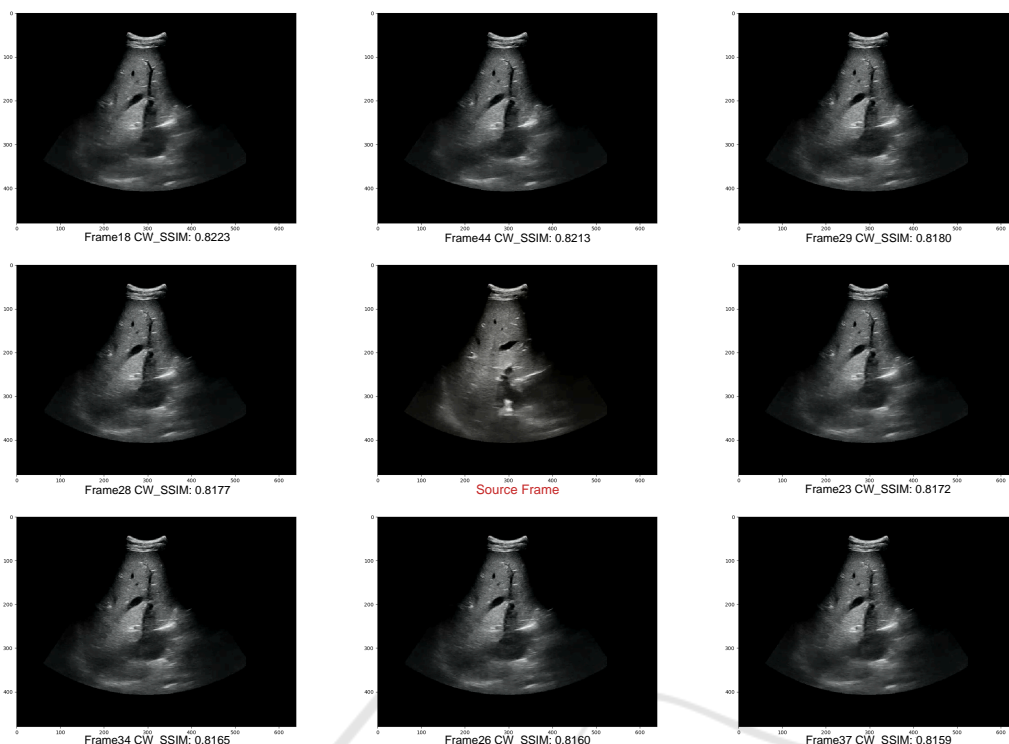


Figure 10: The highest CW-SSIM values compared to the source frame (angle prior to transition) at the +10° angle of the abdomen.

shows the structure on a similar position of the X-axis to allow a smooth change.

Figure 10 shows the 8 frames in the target angle with the highest CW-SSIM values compared to the source frame.

The frames with the smallest change in the +10° degree step of the kidney are all from a similar similarity range. Structural similarity can be appropriate, but would need to be preprocessed ($n \times m$ possibilities in each of the two angular directions).

Another drawback analogous to the tracking problem is the lack of momentum. In the case of the respiration curve, there are several similar CW-SSIM values at the time of inhalation or exhalation, which, unlike optical flow, cannot be distinguished.

5 CONCLUSION

In this work, three systems were presented and evaluated for their suitability for smooth angle change in ultrasound simulators. The calculation of the motion profile using optical flow proved to be successful and can be integrated into simulators. The angle transition is expected to be synchronous in the abdomen as well as with visibility of vessels and is preferable to previous synchronization based on respiratory and pulse

recordings at the time of acquisition, since both artifacts are taken into account.

For future work, the proposed method should be evaluated based on explicit quality criteria and on additional organs. Since ultrasound simulators are rarely open source, it is difficult to directly compare the proposed method with other approaches side by side. Therefore, in the future, there should be efforts to provide an open source ultrasound simulator in which this method can then be applied alongside others. In addition, it would be useful to publish some recordings to generate a benchmark dataset for synchronization of ultrasound recordings. It should also be investigated whether the motion profiles can be useful for diagnostic purposes besides estimating heart rate and respiratory rate.

REFERENCES

Bergen, J. R., Burt, P. J., Hingorani, R., and Peleg, S. (1990). Computing two motions from three frames. In *International Conference on Computer Vision*, volume 90, pages 27–32.

Blum, T., Rieger, A., Navab, N., Friess, H., and Martignoni, M. (2013). A review of computer-based simulators for ultrasound training. *Simulation in Healthcare*, 8(2).

Bolme, D. S., Beveridge, J. R., Draper, B. A., and Lui, Y. M.

- (2010). Visual object tracking using adaptive correlation filters. In *2010 IEEE computer society conference on computer vision and pattern recognition (CVPR)*, pages 2544–2550. IEEE.
- Boukerroui, D., Noble, J. A., and Brady, M. (2003). Velocity estimation in ultrasound images: A block matching approach. In *Biennial International Conference on Information Processing in Medical Imaging*, pages 586–598. Springer.
- Bracewell, R. (1978). *The Fourier Transform and its Applications*. McGraw-Hill Kogakusha, Ltd., Tokyo, second edition.
- Bradski, G. (2000). The opencv library. *Dr. Dobb's Journal of Software Tools*, 25:120–125.
- Horn, B. K. and Schunck, B. G. (1981). Determining optical flow. In *Techniques and Applications of Image Understanding*, volume 281, pages 319–331. International Society for Optics and Photonics.
- Ishii, I., Taniguchi, T., Yamamoto, K., and Takaki, T. (2011). High-frame-rate optical flow system. *IEEE Transactions on Circuits and Systems for Video Technology*, 22(1):105–112.
- Kearney, J. K., Thompson, W. B., and Boley, D. L. (1987). Optical flow estimation: An error analysis of gradient-based methods with local optimization. *IEEE Transactions on Pattern Analysis and Machine Intelligence*, PAMI-9(2):229–244.
- Lawton, D. T. (1983). Processing translational motion sequences. *Computer Vision, Graphics, and Image Processing*, 22(1):116–144.
- Lucas, B. D. and Kanade, T. (1981). An iterative image registration technique with an application to stereo vision. In *Proceedings of the 7th International Joint Conference on Artificial Intelligence - Volume 2, IJCAI'81*, page 674–679, San Francisco, CA, USA. Morgan Kaufmann Publishers Inc.
- Lukežič, A., Vojří, T., Čehovin Zajc, L., Matas, J., and Kristan, M. (2018). Discriminative correlation filter tracker with channel and spatial reliability. *International Journal of Computer Vision*, 126(7):671–688.
- Matej, K. et al. (2016). The visual object tracking vot2016 challenge results. In *European Conference on Computer Vision (ECCV) Workshops*.
- Ourahmoune, A., Larabi, S., and Hamitouche-Djabou, C. (2012). A survey of echographic simulators. In Giamberardino, P. D., Iacoviello, D., Tavares, J. M. R. S., and Jorge, R. M. N., editors, *Computational Modelling of Objects Represented in Images - Fundamentals, Methods and Applications III, Third International Symposium, CompIMAGE 2012, Rome, Italy, September 5-7, 2012*, pages 273–276. CRC Press.
- Pan, J. and Tompkins, W. J. (1985). A real-time qrs detection algorithm. *IEEE transactions on biomedical engineering*, BME-32(3):230–236.
- Puybareau, E., Talbot, H., and Léonard, M. (2015). Automated heart rate estimation in fish embryo. In *2015 International Conference on Image Processing Theory, Tools and Applications (IPTA)*, pages 379–384. IEEE.
- Roffo, G., Kristan, M., Matas, J., Felsberg, M., Pfugfelder, R., Cehovin, L., Vojjir, T., Hager, G., Melzi, S., and Fernandez, G. (2016). The visual object tracking vot2016 challenge results. In *Proceedings of the IEEE European Conference on Computer Vision Workshops (ECCV), Amsterdam, The Netherlands*, pages 8–16.
- Sampat, M. P., Wang, Z., Gupta, S., Bovik, A. C., and Markey, M. K. (2009). Complex wavelet structural similarity: A new image similarity index. *IEEE transactions on image processing*, 18(11):2385–2401.
- Wang, Z., Bovik, A. C., Sheikh, H. R., and Simoncelli, E. P. (2004). Image quality assessment: from error visibility to structural similarity. *IEEE transactions on image processing*, 13(4):600–612.
- Wu, Y., Lim, J., and Yang, M. (2015). Object tracking benchmark. *IEEE Transactions on Pattern Analysis and Machine Intelligence*, 37(9):1834–1848.
- Xu, K., Gábor Csapó, T., Roussel, P., and Denby, B. (2016). A comparative study on the contour tracking algorithms in ultrasound tongue images with automatic re-initialization. *The Journal of the Acoustical Society of America*, 139(5):EL154–EL160.